Electronic Supplementary Material (ESI) for Physical Chemistry Chemical Physics.

Supporting information

1 Determination of T*

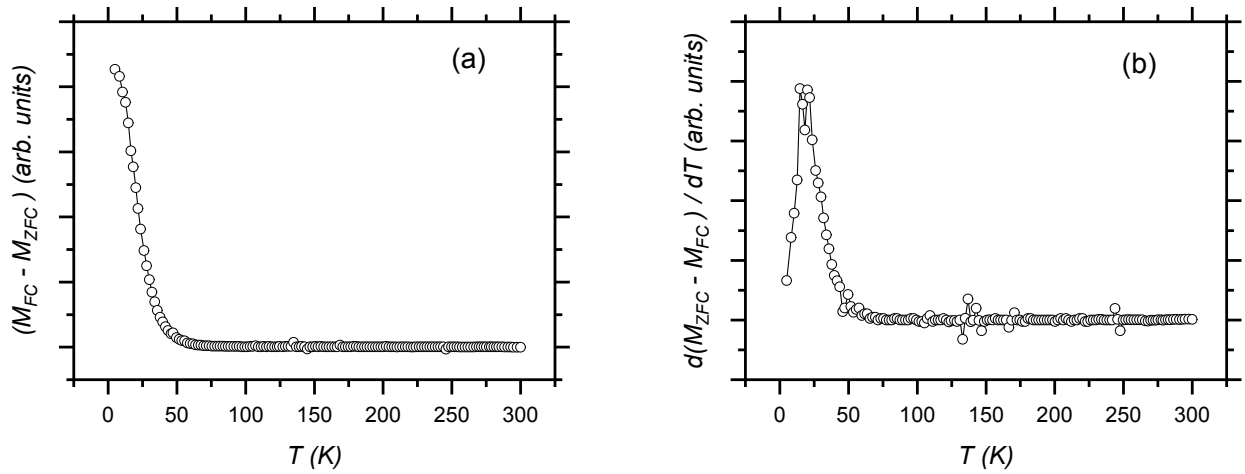

Fig. S1. (M_{FC}-M_{ZFC}) curve (a) measured after a field cooling with an applied field of 2.5 mT for sample S17. Panel (b) shows the respective negative derivative, proportional to the blocking energy distribution of the sample.

2 Characterization of CFO and CNFO samples

2.1 Structure and Morphology

The XRD patterns of both samples (**Fig. S2**) exhibit the common reflexes of a spinel structure with cubic close packaging of oxygen ions. No other phases are detected. The results from TEM images analysis (**Fig. S3**) show strongly aggregated particles, which homogenous size and almost spherical shape.

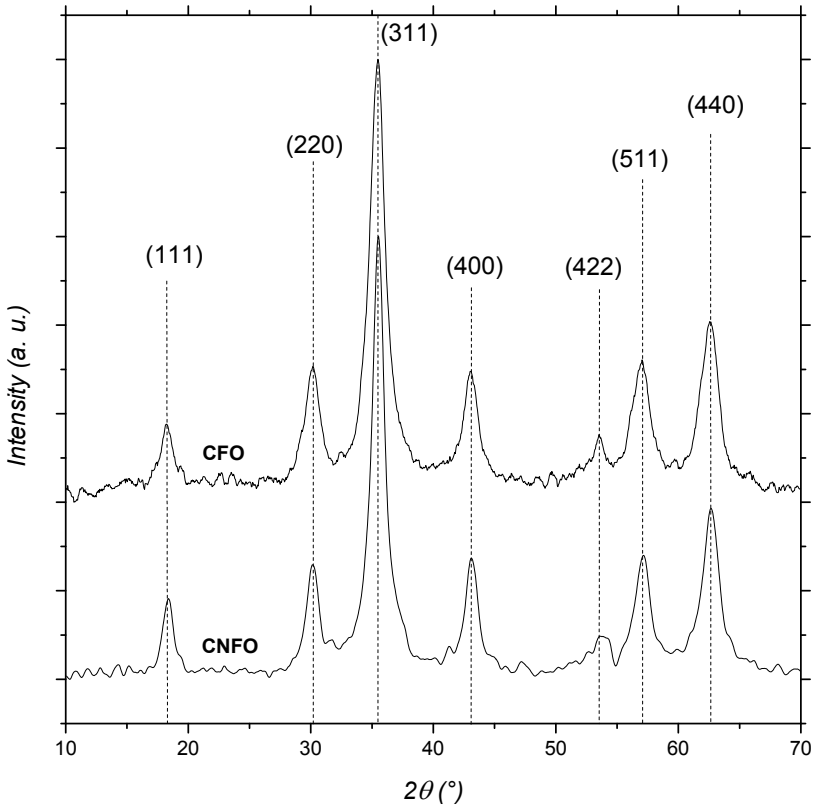

Fig. S2. XRD pattern of the two samples. All peaks are indexed as FCC spinel ferrite reflections.

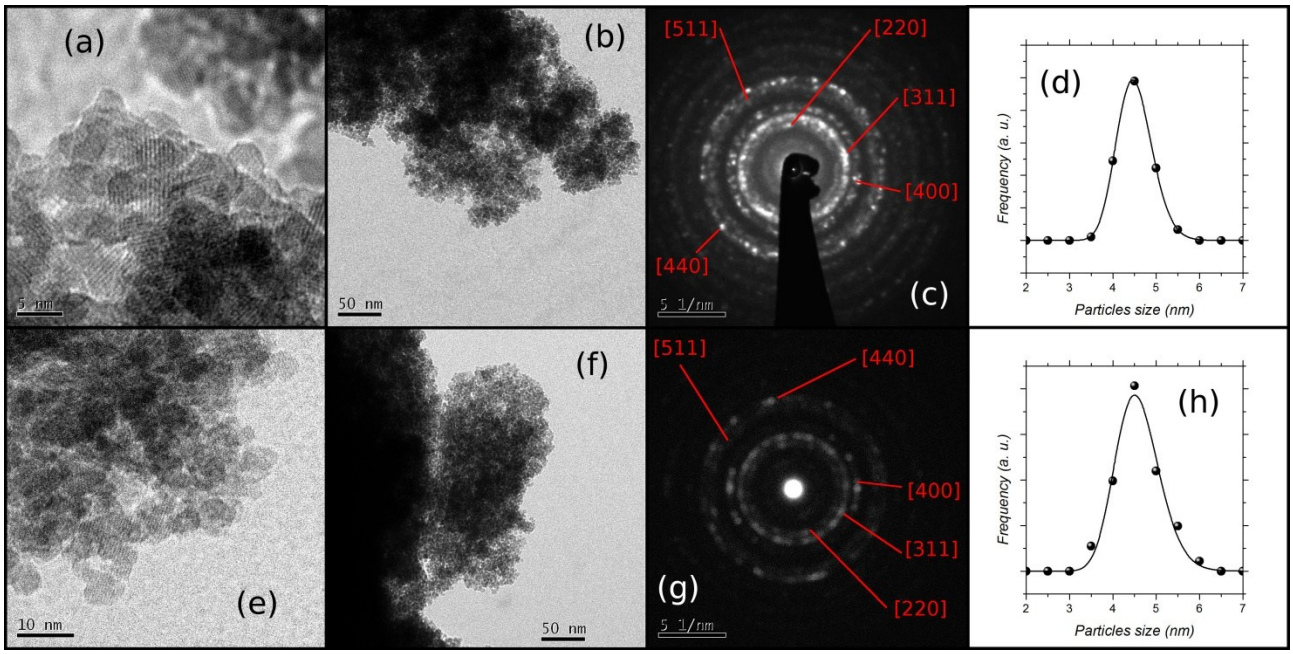

Fig. S3. TEM images of sample CFO (a and b) and CNFO (e and f) are reported. The spinel crystalline structure is confirmed also by electron diffraction images visible in (c) and (g) for CFO and CNFO, respectively. Particles size distribution are reported in panels (d) (CFO) and (h) (CNFO).

2.2 Molecular Coating

In order to study the interaction of triethylene glycol (TEG) on nanoparticles (NPs) we have analyzed the FT-IR spectra of the samples (**Fig. S4**). FT-IR spectra were collected in the region from 400 to 4000 cm^{-1}, using a Bruker Equinox 55 spectrophotometer. NPs were analyzed dispersing powders in KBr pellets, or for liquids, using a drop over pure KBr pellets.

The presence of spinel ferrite structure is confirmed by the signals around 590 cm^{-1}, referred to the stretching vibration of the metal in tetrahedral site and the oxygen, while the signal around 406 cm^{-1} (partially visible) is the analogous for metal in octahedral site[1,2]. The symmetrical and asymmetrical stretching of C-H (with signals between 2937 and 2868 cm^{-1}), and of C-O (around 1100 cm^{-1}) confirm the polyol coating presence in all samples [3]. In particular, the interaction between polyol oxygen and metal cations at particles surface is shown by both the small shift to lower frequencies of the C-O signals with respect to the pure polyol [4], and in their different intensity profile [5,6] (i.e., two signals replace the three of the pure TEG). The signals around 3400 and at 1646 cm^{1} are referred respectively to the stretching and bending modes of O-H of polyol and adsorbed water[3]. In all spectra, the signal around 1646 cm^{1} is coupled with a second one shifted to a lower value, that can be attributed to the water linked to particles surface or on polyol bonded on the surface[7]. Finally, the complex profile between 1450 and 1250 cm^{-1}, produced by C-H bending [8], has different intensity and profile with respect free TEG, as results of interactions between polyol and NP surface.

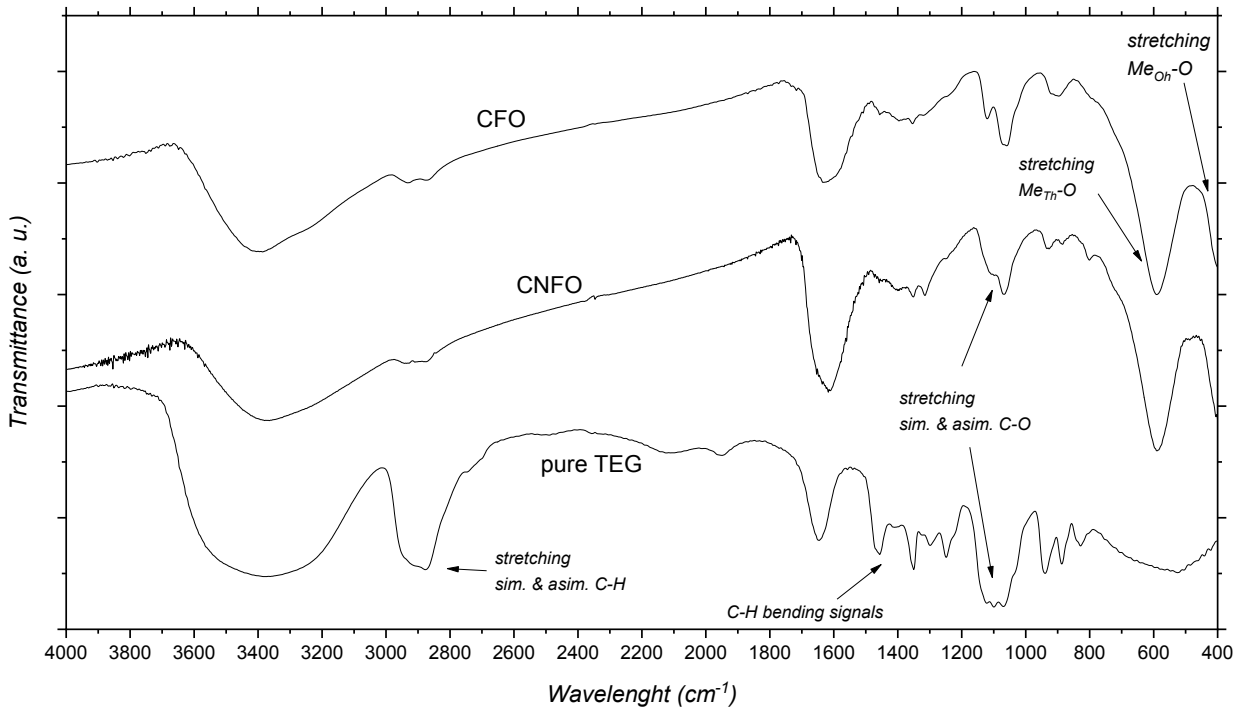

Fig. S4. FT-IR spectra of the samples and pure TEG for comparison.

Fig. S5 compares the TGA-SDTA curves of all samples. TGA-SDTA measurements were performed using a Mettler-Toledo TGA/SDTA 851. Data were collected in the range 25-1000°C with a heating rate of 10°C min^{-1} under oxygen flow (flow rate of 50 ml/min). For each one, the evaporation of residual water and acetone manifests as a small loss in weight with a corresponding endothermic event, completed around 100 °C. The successive main loss around 250 °C is coupled with an exothermic peak, and it is due to decomposition of TEG (decomposition temperature centered at 247 °C for pure TEG). CFO shows the corresponding DTA peak centered around 250°C; for CNFO this peak becomes bigger, reflecting the larger amount of adsorbed TEG, and it moves toward 240°C.

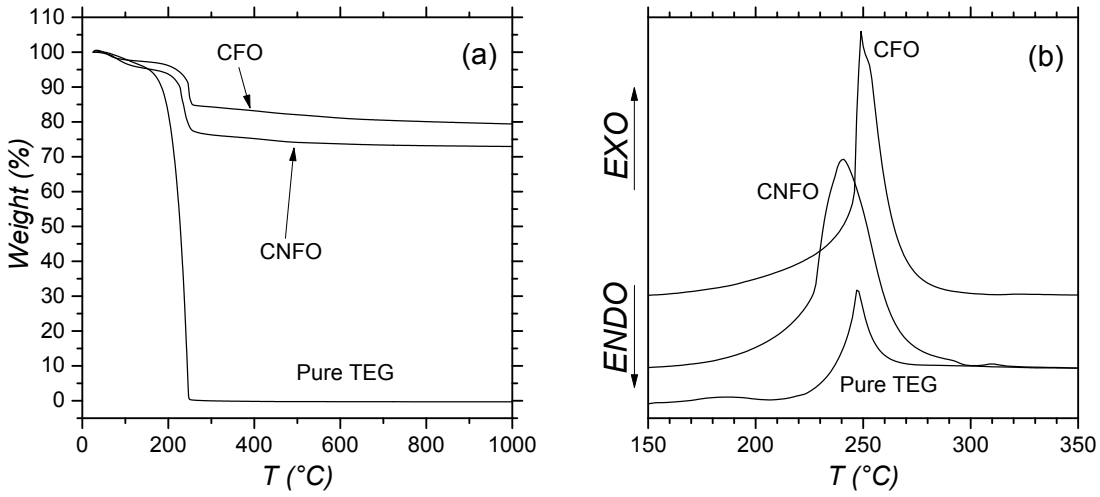

Fig. S5: Panel (a) reports TGA curves for both samples and for the pure TEG. The corresponding SDTA curves are shown in the region around 250°C, in panel (b).

3 Interparticle interactions

The field dependence of the remanent magnetization was measured using the IRM (Isothermal Remanent Magnetization) and DCD (Direct Current Demagnetization) protocols. According to the IRM protocol, the samples, in the demagnetized state, were cooled in a zero magnetic field down to 5 K. At this temperature, a small external field was applied for 10 s, then switched off, and finally the remanence (M_{IRM}) was measured. The process was repeated, increasing the field in steps up to 5 T. In a DCD measurement, the initial state was the magnetically saturated one. After cooling the sample at 5 K, an external field of −5 T was applied for 10 s, then it was turned off and the remanence (M_{DCD}) was measured. As in IRM, a small external field was applied in the opposite direction to magnetization for 10 s and then switched off, and the remanent magnetization was measured. This was repeated increasing the field up to +5 T.

The analysis of the remanent magnetization curves measured by *IRM* and *DCD* protocols allows us to investigate the interaction regime among particles. For an assembly of non-interacting single-domain particles with uniaxial anisotropy and magnetization reversal by coherent rotation, the two remanence curves are related via the Wohlfarth equation [9]:

$$m_{DCD}(H) = 1 - 2m_{IRM}(H) \qquad (1)$$

where $m_{DCD}(H)$ and $m_{IRM}(H)$ represent the reduced terms $M_{DCD}(H)/M_{DCD(5T)}$ and $M_{IRM}(H)/M_{IRM(5T)}$, and $M_{DCD(5T)}$ *and* $M_{IRM(5T)}$ are the remanence values for the *DCD* and *IRM* curves for a reverse field of 5 T, respectively. Kelly et al. [10] rewrote the Wohlfarth equation to explicitly reveal deviations from a non-interacting case:

$$\Delta M = m_{DCD}(H) - 1 + 2m_{IRM}(H) \qquad (2)$$

Negative *ΔM*, as those observed in **Fig. 5** for the CFO and CNFO, are usually taken as indicative of the prevalence of demagnetizing (e.g., dipole-dipole) interactions; positive values are attributed to interactions promoting the magnetized state (e.g., direct exchange interactions). Qualitatively, the intensity of such deviation ($I_{\Delta M}$) can be considered proportional to the strength of the interparticles interactions, anyway, the analysis can be further improved calculating a mean value of interactions field between the particles. Following equation (1), the two irreversible susceptibilities (χ_{irr} = d*m*/d*H)* are related as:

$$\left|\frac{dm_{DCD}}{dH}\right| = 2\frac{dm_{IRM}}{dH} \qquad (3)$$

with a maximum at the same reverse field. Deviations from such behavior are due to the presence of interactions which can be quantified in terms of the so-called interaction field [11]:

$$H_{int} = \frac{\left(H_r^{DCD} - H_r^{IRM}\right)}{2} \qquad (4)$$

$H_r^{DCD}$and H_r^{IRM} correspond to the position of the maxima of the field derivative of $m_{DCD}(H)$ and $m_{IRM}(H)$ curves.

References

1 A. Baykal, H. Deligöz, H. Sozeri, Z. Durmus and M. S. Toprak, Triethylene Glycol Stabilized CoFe2O4 Nanoparticles, *J. Supercond. Nov. Magn.*, 2012, **25**, 1879–1892.

2 C. Cannas, a. Ardu, a. Musinu, D. Peddis and G. Piccaluga, Spherical Nanoporous Assemblies of Iso-Oriented Cobalt Ferrite Nanoparticles: Synthesis, Microstructure, and Magnetic Properties, *Chem. Mater.*, 2008, **20**, 6364–6371.

3 W. Cai and J. Wan, Facile synthesis of superparamagnetic magnetite nanoparticles in liquid polyols., *J. Colloid Interface Sci.*, 2007, **305**, 366–70.

4 H. Deligöz, A. Baykal, E. E. Tanrıverdi, Z. Durmus and M. S. Toprak, Synthesis, structural and electrical properties of triethylene glycol (TREG) stabilized Mn0.2Co0.8Fe2O4 NPs, *Mater. Res. Bull.*, 2012, **47**, 537–543.

5 H. Yang, C. Zhang, X. Shi, H. Hu, X. Du, Y. Fang, Y. Ma, H. Wu and S. Yang, Water-soluble superparamagnetic manganese ferrite nanoparticles for magnetic resonance imaging., *Biomaterials*, 2010, **31**, 3667–3673.

6 M. Günay, H. Erdemi, A. Baykal, H. Sözeri and M. S. Toprak, Triethylene glycol stabilized MnFe2O4 nanoparticle: Synthesis, magnetic and electrical characterization, *Mater. Res. Bull.*, 2013, **48**, 1057–1064.

7 G. Velazquez, A. Herrera-Gómez and M. O. Martín-Polo, Identification of bound water through infrared spectroscopy in methylcellulose, *J. Food Eng.*, 2003, **59**, 79–84.

8 D. Maity, S. N. Kale, R. Kaul-Ghanekar, J.-M. Xue and J. Ding, Studies of magnetite nanoparticles synthesized by thermal decomposition of iron (III) acetylacetonate in tri(ethylene glycol), *J. Magn. Magn. Mater.*, 2009, **321**, 3093–3098.

9 E. P. Wohlfarth, Relations between Different Modes of Acquisition of the Remanent Magnetization of Ferromagnetic Particles, *J. Appl. Phys.*, 1958, **29**, 595–596.

10 K. O'Grady and R. W. Chantrell, Remanence Curves of Fine particles Systems I: Experimental Studies.

11 X. Batlle, M. Del Muro and A. Labarta, Interaction effects and energy barrier distribution on the magnetic relaxation of nanocrystalline hexagonal ferrites, *Phys. Rev. B*, 1997, **55**, 6440–6445.